Microstructure, Luminescence, and Stability of a Europium Complex Covalently Bonded to an Attapulgite Clay

ARTICLE *in* THE JOURNAL OF PHYSICAL CHEMISTRY B · OCTOBER 2009

Impact Factor: 3.3 · DOI: 10.1021/jp906848e · Source: PubMed

6 AUTHORS, INCLUDING:

Yufei Ma
Chinese Academy of Sciences
23 PUBLICATIONS **216** CITATIONS
SEE PROFILE

Yu Tang
Lanzhou University
96 PUBLICATIONS **858** CITATIONS
SEE PROFILE

Microstructure, Luminescence, and Stability of a Europium Complex Covalently Bonded to an Attapulgite Clay

Yufei Ma, Haiping Wang, Weisheng Liu, Qiong Wang, Jun Xu, and Yu Tang*

College of Chemistry and Chemical Engineering, State Key Laboratory of Applied Organic Chemistry, Lanzhou University, Lanzhou 730000, People's Republic of China

Received: July 20, 2009; Revised Manuscript Received: September 8, 2009

Attapulgite clay, natural silicate nanorods, can form nanocomposites with extreme chemical stability and remarkable exposure durability. Combining luminescent lanthanide complexes with attapulgite to improve their stability and even luminescent properties is fascinating, promising but challenging in the lanthanide composite field. A europium complex $Eu(tta)_3(H_2O)_2$ (Htta = 2-thenoyltrifluoroacetone) was covalently coupled on attapulgite (and MCM-41 or ZSM-5 for comparison) via ligand exchange reaction, generating the first example of attapulgite-based ternary europium complexes. The composites were characterized by ^{29}Si magic-angle spinning (MAS) NMR, CHN elemental analysis, inductively coupled plasma-atomic emission spectroscopy (ICP) for Eu^{3+} contents, X-ray diffraction (XRD), and UV−vis absorption spectra. The results indicate that Eu^{3+} complexes bond covalently to the outer surfaces of attapulgite, permeate the channels, and are stuck with the complexes bonded to the inner walls of the pores in MCM-41, or invade into the channels of ZSM-5 after decomposition. These structures were further evidenced by luminescence efficiency and coordinated waters of the complexes linked to matrixes. The composites display more efficient emission, enhanced thermal stability, and improved exposure durability in comparison with the isolated complexes, due to interactions of the complexes with the matrixes. The most efficient emission of attapulgite-based complexes among the composites results from the uniformly structured ternary europium complexes.

Introduction

Lanthanide-containing composites have drawn much attention for the past decade because of their wide application for display and lighting devices.[1−4] They combine the outstanding luminescent properties (such as large Stokes shifts, long radiative lifetimes, and narrow emission bands) and tolerability of lanthanide complexes with the remarkable stability of various hosts, including polymers,[2,5,6] xerogels,[4,7] zeolites,[8] mesoporous materials,[9−11] TiO_2[12] or α-ZrP,[13] liquid crystals,[3,14] and even carbon nanotubes[15] or clays.[16] As the existing literatures illustrated, complexes encapsulated in a matrix led to an enhanced stability compared with the isolated complexes under heat or UV light due to interaction of the complexes with the matrix structure; moreover, stronger interactions generated more satisfied luminescent properties and higher stability.

Attapulgite (so-called palygorskite) is a natural clay mineral of nanoscaled fibrous hydrous magnesium silicates. Its structure can be described as two bands of silica tetrahedra linked by magnesium ions in octahedral coordination and capillary channels (about 3.4 Å × 6.4 Å wide) due to the absence of the alternating positions of the apical oxygen in the tetrahedral layers.[17] Attapulgite is famous for Maya blue, a nanocomposites combining attapulgite with indigo dye,[18] which has been confounding researchers for its extreme chemical stability and remarkable exposure durability for decades[17−19] and remains a mystery.[20] Encouraged by Maya blue, researchers prepared some clay-based lanthanide complexes,[16,21−23] seeking for stable and luminescent composites with potential lighting and displaying application. However, the preparation is much challenging since the natural clay needs careful purification to procure silicate nanorods (in case of attapulgite) and suitable modification to be further functionalized; besides, the irregular structures of the clay-based complexes are hardly analyzed due to the complicated compositions in the natural clays. As a result, only a few literatures about clay-based lanthanide composites have been reported,[16,21−23] focusing on the photoluminescent complexes encapsulated only by weak interactions in the matrixes, mostly montmorillonite.[16,22−24] However, most of these composites are weakly luminescent and disorderly structured.

Herein we discuss the preparation and luminescence of a europium complex covalently attached to attapulgite. To our best knowledge, this is the first example of loading lanthanide complexes covalently onto the clay. In order to investigate the microstructure and stability of the attapulgite-based europium complexes, other widely used matrixes were chosen for comparison, such as MCM-41 owing to its relatively large pore (2−3 nm) and ZSM-5 because of its small pore[25] (5.5 Å × 5.6 Å) similar to the channel of attapulgite. The resulting attapulgite-based composites form a uniform ternary europium complex emitting bright red light and possess enhanced stability under UV light or heat.

Experimental Section

Materials. 3-(Aminopropyl)triethoxysilane (APTES, 99%) was a reagent of Acros Organics. Kaiser test reagents were prepared according to the literature.[26] Europium chloride ($EuCl_3 \cdot 6H_2O$) was obtained by dissolving Eu_2O_3 (99.99%, Shanghai Yuelong) in hydrochloric acid followed by successive fuming to remove excess acid. 2-Thenoyltrifluoroacetone (Htta, AR), 1,10-phenanthroline (AR), and the other chemicals were all commercially available and used as received.

Attapulgite (Atta), purchased from Gansu Kaixi Corporation Limited, was purified through dispersion into $(NaPO_3)_6$ aqueous

* To whom correspondence should be addressed. Tel.: +86-931-8912552. Fax: +86-931-8912582. E-mail: tangyu@lzu.edu.cn.

10.1021/jp906848e CCC: $40.75
Published on Web 10/07/2009

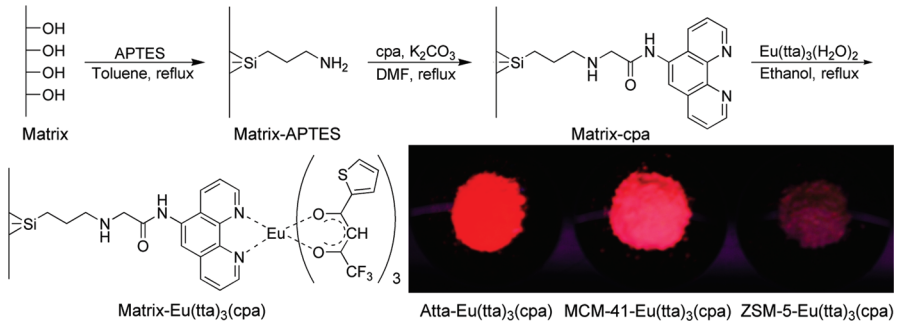

Figure 1. Synthesis procedure and predicted structure of matrix−Eu(tta)$_3$(cpa). The photography shows the composites under UVA irradiation (365 nm).

solution, followed by treating with HCl and H_2O_2. The resulting white clay was finally dispersed in benzene (25 g·L^{-1}) as stock solution. MCM-41 (2.5 nm pore size) was synthesized according to the literature.[27] ZSM-5 was purchased from Nankai University Catalyst Company and used without any purification.

Synthesis of 2-Chloro-*N*-(1,10)-phenanthroline-5-yl-acetamide (cpa). 5-Amino-(1,10)-phenanthroline (428 mg, 2.0 mmol, prepared by nitration of 1,10-phenanthroline and then reduction of the nitro derivative according to the literature[28,29]) and $NaHCO_3$ (255 mg, 3.0 mmol) were dispersed in 10 mL of anhydrous CH_3CN. The suspension was cooled to 0 °C before chloroacetyl chloride (178 mg, 2.2 mmol) in 10 mL of anhydrous CH_3CN was added dropwise. After stirring for 4 h at room temperature, 480 mg of the resulting yellow solid was obtained after filtering off, washing with ethanol, and drying at 60 °C. ^{1}H NMR ($CDCl_3$): δ = 9.25 (d, 4.4 Hz, 1H), 9.17 (d, 4.4 Hz, 1H), 8.88 (bs, 1H), 8.38 (s, 1H), 8.31 (d, 8.4 Hz, 1H), 8.26 (d, 8.0 Hz, 1H), 7.73 (dd, 4.4 Hz, 8.4 Hz, 1H), 7.65 (dd, 4.4 Hz, 8.0 Hz, 1H), 4.41 (s, 2H). ^{13}C NMR ($CDCl_3$): δ = 164.2, 150.0, 149.8, 146.1, 144.2, 138.9, 137.2, 135.6, 128.5, 127.6, 123.2, 122.6, 119.2, 26.5.

Synthesis of Eu(tta)$_3$(cpa). Solid cpa (27.1 mg, 0.10 mmol) was mixed with 25 mL of 95% ethanolic solution of Eu(tta)$_3$(H_2O)$_2$ (85.2 mg, 0.30 mmol, prepared from Htta and $EuCl_3$·6H_2O following the literature[30]), and then the suspension was sonicated to completely dissolve cpa and filtered. An amount of 25 mL of water was added to the filtrate, following by filtering off the resulting solid. The pale pink solid was washed with ethanol−water (v/v = 1:1) and dried in vacuum at room temperature, obtaining 72.0 mg of Eu(tta)$_3$(cpa). Elem. Anal. Calcd: C, 41.98; H, 2.04; N, 3.86; Eu, 17.85. Found: C, 42.11; H, 2.21; N, 3.42; Eu, 17.81.

Silylation of Matrixes. As described in Figure 1, 500 mg of matrix (matrix = Atta, MCM-41, and ZSM-5) in 50 mL of toluene mixing with 1 mL of APTES was stirred and refluxed for 8 h. The solid was then separated by centrifugation, washed with toluene and ethanol after sonication for 30 min, and dried at room temperature. The APTES silylation of MCM-41 has been reported.[9] Transmission electron microscopy (TEM) images (Supporting Information Figure S1) show that Atta−APTES maintains rodlike morphology (10−20 nm wide, 100−500 nm long).

Synthesis of Matrix−cpa. The sample of matrix−APTES (500 mg) and K_2CO_3 (138 mg, 1.0 mmol) were suspended in 30 mL of dimethylformamide (DMF), sonicated for 30 min, and then 20 mL of DMF containing cpa (271 mg, 1.0 mmol) was added. The mixture was refluxed for 24 h and centrifuged. Through washing the resulting solids with DMF and ethanol and drying at room temperature, the 1,10-phenanthroline-functionalized matrix, matrix−cpa sample was obtained.

Synthesis of the Matrix−Eu(tta)$_3$(cpa) Complexes. A batch of 500 mg of matrix−cpa was refluxed with 50 mg of Eu(tta)$_3$(H_2O)$_2$ in ethanol. The suspension was collected by centrifugation after 24 h, and the excess of unbounded complexes were thoroughly washed away with ethanol until no red emission of the washing solution was witnessed under the UV excitation (254 nm). Dried at 120 °C for 3 h, matrix−Eu(tta)$_3$(cpa) emitting bright red light under UVA (365 nm) irradiation (Figure 1) was obtained. The composites contained 2−3 wt % Eu elements (detailed in Table S1, see the Supporting Information).

Characterization. ^{1}H NMR and ^{13}C NMR spectra were recorded on a Varian Mercury-300B spectrometer; solid-state ^{29}Si magic-angle spinning (MAS) NMR spectra were performed at 79.46 MHz, using a Bruker Ultrashield 400 plus spectrometer. CHN elemental analyses were measured on an Elementar Vario EL analyzer; the contents of Eu^{3+} ion were obtained by inductively coupled plasma-atomic emission spectroscopy (ICP) using an IRIS Advantage ER/S spectrophotometer. Fourier transform infrared (FTIR) spectra were conducted within the 4000−400 cm^{-1} wavenumber range using a Nicolet 360 FTIR spectrometer with the KBr pellet technique. Transmission electron microscope images were taken on a JEM-100CX II apparatus. X-ray diffraction patterns (XRD) were determined with Rigaku-Dmax 2400 diffractometer using Cu Kα radiation. The UV−vis absorption spectra were recorded on a Perkin-Elmer Lambda 950 spectrophotometer. The steady-state luminescence spectra and the lifetime measurements were measured on an Edinburgh Instruments FSL920 fluorescence spectrometer, with a 450 W Xe arc lamp as the steady-state excitation source or a Nd-pumped OPOlette laser as the excitation source for lifetime measurements; in the experiments of photoluminescent stability, monochromic light (350 nm) separated from the 450 W Xe arc lamp was used as the irradiation source, with a slit of 0.8 nm and a shutter opening after 10 s for 800 s. Thermogravimetric (TG) analysis was performed on a Perkin-Elmer thermal analyzer up to 750 °C at a heating rate of 5 °C/min (<300 °C) and then 10 °C/min (>300 °C) under static air. Additional heat treatments were carried out at various temperatures (120−240 °C) for 0.5 h in air.

Results and Discussion

Characterization of Composition and Microstructure. ^{29}Si MAS NMR spectroscopy results of the matrix−APTES samples are displayed in Figure 2. The peaks related to the organosiloxane T^n (T^n = RSi(OSi)$_n$OH$_{3-n}$, n = 1−3) and siloxane Q^m (Q^m = Si(OSi)$_m$(OH)$_{4-m}$, m = 2−4) species can be clearly identified. The dominance of T^3 (−64 and −67 ppm for Atta−APTES, and −65 ppm for MCM-41−APTES) NMR signals suggests that the hydrolysis and condensation of APTES

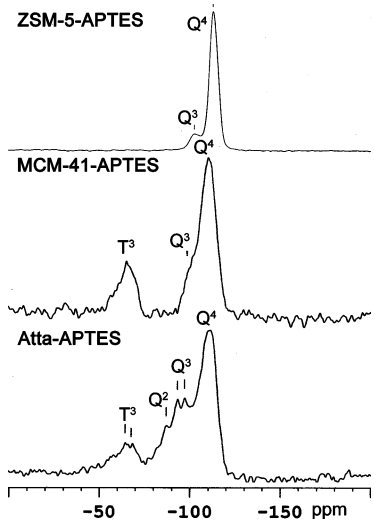

Figure 2. ^{29}Si MAS NMR spectra of matrix−APTES samples.

on the surfaces of the matrixes are nearly complete, resulting in a strong linkage (three Si−O−Si covalent bonds) between APTES and the matrixes. No obvious T^n peak in ZSM-5−APTES was found, maybe because only a small amount of Si−OH is on the surface of ZSM-5 (Q^3 peak at 102 ppm may be from the inside channels). For MCM-41−APTES, the relatively low intensity of Q^3 (−99 ppm) in comparison with Q^4 (−110 ppm) indicates the minority of the Si−OH groups on the surfaces after silylation, which is a better result compared with the literature of the same purpose.[9] Q^2 (−87 ppm) and Q^3 (−93, −97 ppm) peaks in Atta−APTES may be assigned to the Si−OH groups inside the channels, whereas APTES is covalently bonded onto the outer surfaces of Atta. Because some Al (or Mg) atoms take the places of Si atoms in attapulgite, T^3 and Q^3 signals both display two peaks.

The presence or absence of primary amine groups on the surface of modified materials can be confirmed by using a Kaiser test according to literatures.[26,31] The samples untreated or treated with APTES were suspended in ethanol. After two drops of each Kaiser test reagent (phenol, potassium cyanide, and ninhydrin) were added, the suspensions were heated in a boiling water bath for a few minutes. The APTES-treated suspensions should turn deep blue, whereas the untreated samples might remain slightly pale yellow, because this blue color is indicative of the reaction of ninhydrin with free primary amine groups present in the suspension.[31] Matrix−APTES showed deep blue color, whereas bare matrixes and matrix−cpa samples displayed yellow and pale blue color, respectively. The results suggest the successful APTES silylation of the matrixes and sharp decreases of NH_2 amounts in matrix−APTES samples because of the formation of matrix−cpa.

It is of little possibility to predict the forms of the matrix−Eu(tta)$_3$(cpa) complexes in the FTIR spectra (Figure S2, see the Supporting Information). This is because of the low amount of Eu(tta)$_3$(cpa) complexes incorporated in the matrix, and consequently the domination of the strong Si−O−Si framework vibrations (υ_{as}(Si−O) at ∼1086 cm^{-1}, and δ(Si−O−Si) at ∼462 cm^{-1}). Si−OH, which might be evidenced by δ(O−H) at 3616 cm^{-1}, exists in Atta−Eu(tta)$_3$(cpa) and ZSM-5−Eu(tta)$_3$(cpa), whereas no such evidence appears in MCM-41−Eu(tta)$_3$(cpa). The peak at 3542 cm^{-1} can be ascribed to the coordination water in the channels of Atta−Eu(tta)$_3$(cpa). These results are in consistent with the results in the ^{29}Si MAS NMR spectra.

In the XRD patterns of matrix−Eu(tta)$_3$(cpa) samples (Figure S3 in the Supporting Information), the lack of diffraction peaks

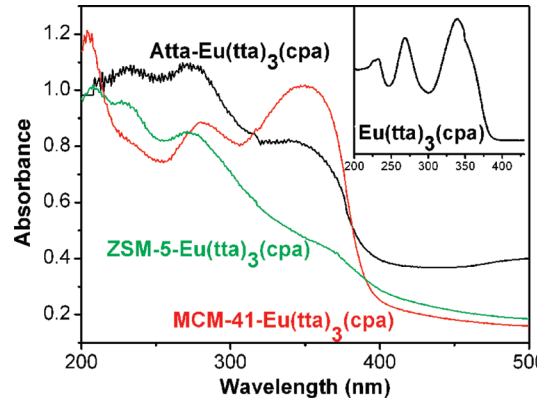

Figure 3. UV−vis absorption spectra of matrix−Eu(tta)$_3$(cpa) samples. The inset shows the absorption spectrum of Eu(tta)$_3$(cpa) in ethanol (2.0×10^{-5} mol·L^{-1}).

SCHEME 1: Schematic Drawing of Atta−Eu(tta)$_3$(cpa) (Red Groups Represent Eu Complexes), MCM-41−Eu(tta)$_3$(cpa), and ZSM-5−Eu(tta)$_3$(cpa)[a]

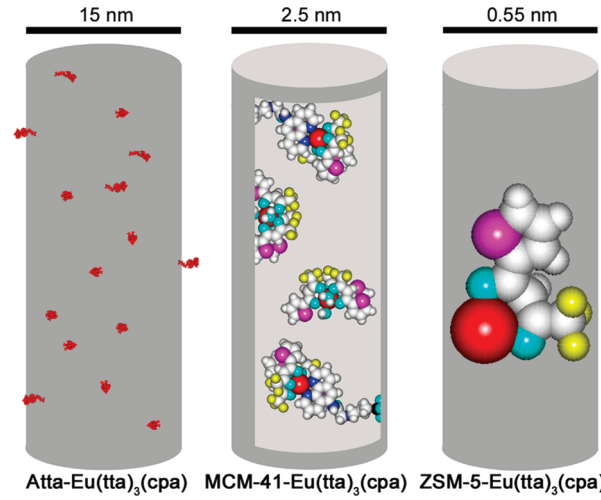

[a] Color code: Eu, red; N, blue; O, cyan; S, violet; F, yellow; Si, black; C and H, white.

in all samples is due to the highly dispersed Eu^{3+} complexes bonded on matrix. Besides, the characteristic patterns of Eu(tta)$_3$(H$_2$O)$_2$ (7.9°, 8.9°, 23.3°, 23.7°, and 24.4°) are also found in MCM-41−Eu(tta)$_3$(cpa), which suggests that some free binary complexes may be trapped in the pore of MCM-41 by APTES and ternary complexes anchored on the wall of the pore.

The absorption spectra of matrix−Eu(tta)$_3$(cpa) samples are displayed in Figure 3. Atta− and MCM-41−Eu(tta)$_3$(cpa) show a wide absorption band at 350 nm, which is similar to that of Eu(tta)$_3$(cpa) or Eu(tta)$_3$(H$_2$O)$_2$ (not shown), indicating that the complexes are embedded in the two matrixes. However, no such similarity is found in ZSM-5−Eu(tta)$_3$(cpa) but a slight shift to 360 nm, we deduce that no such complexes exist in ZSM-5 (that is, neither inside its inner pores nor on the outer surfaces).

The pore size of the matrix can be applied to rationalize the observed facts for the matrix−Eu(tta)$_3$(cpa) samples (as shown in Scheme 1). Eu^{3+} complexes are linked covalently onto the outer surfaces of Atta, due to that its pore (3.4 Å × 6.4 Å)[17] is too little to be penetrated for a Eu(tta)$_3$(H$_2$O)$_2$ molecule (about 8 Å × 15 Å, calculated by the geometry optimization with molecular mechanics method in Hyperchem 7.0) or even for a small molecule like indigo.[20] For MCM-41, the pore (2.5 nm) may hardly accommodate more than one Eu^{3+} complex molecule; therefore, some free Eu(tta)$_3$(H$_2$O)$_2$ molecules permeated

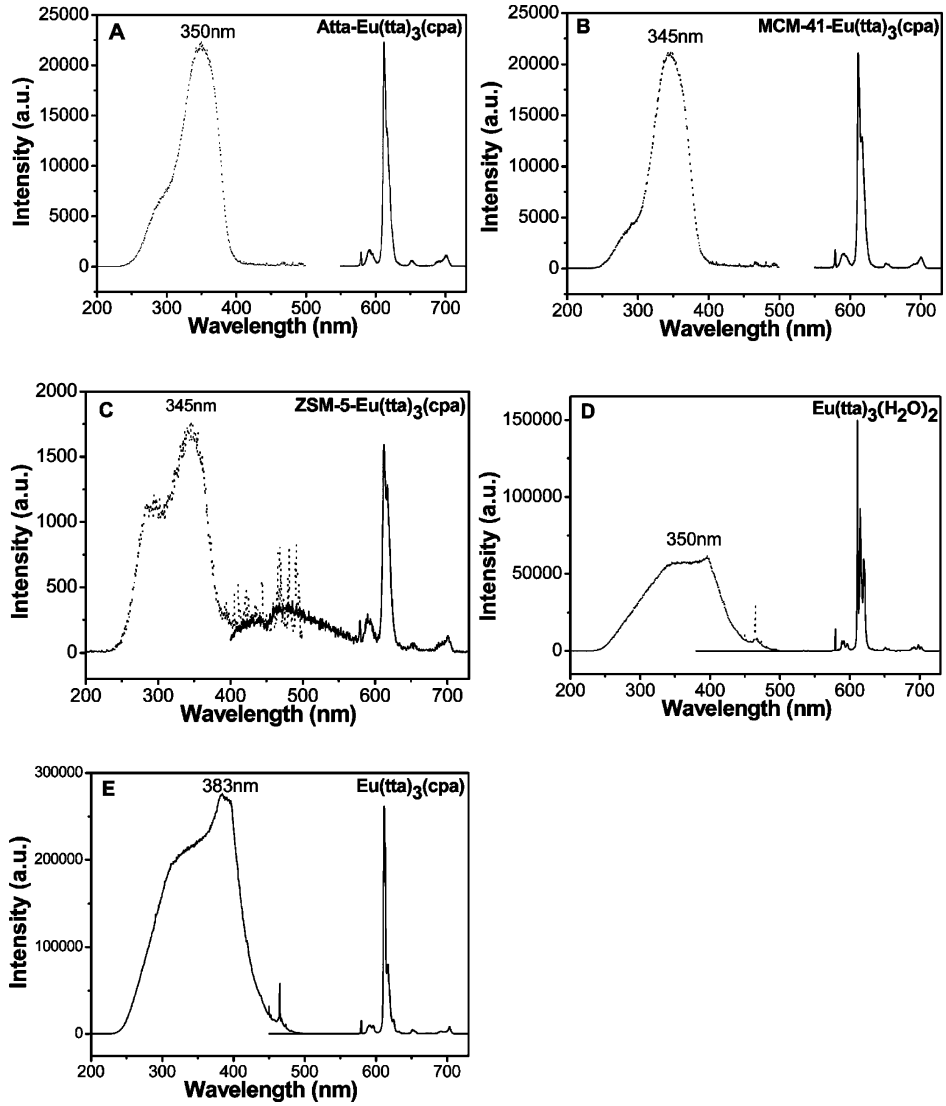

Figure 4. Excitation (dotted lines, monitored at 612 nm) and emission (solid lines, monitored at the maximum excited wavelength which are labeled in the excitation spectra) spectra of the composites (A−C) and isolated complexes (D and E). The excitation and emission slits are 0.25 nm.

the channel are stuck with the ternary complexes (about 9 Å × 20 Å, calculated by the geometry optimization with molecular mechanics method in Hyperchem 7.0) and APTES anchoring on the inner walls of the pores.[9] In ZSM-5, its small channels (5.5 Å × 5.6 Å) and the lack of Si−OH groups on its exterior surfaces complicate the situation. A possibility is that Eu^{3+} complexes might decompose and the incomplete complexes invade into the channels of ZSM-5. As was suggested,[25] the assumption can be proved by the unexpectedly low amount of C contents when comparing the C/Eu molar ratio of ZSM-5−$Eu(tta)_3(cpa)$ (28) with that of Atta−$Eu(tta)_3(cpa)$ (42) or MCM-41−$Eu(tta)_3(cpa)$ (74). However, the presence of a little amount of $Eu(tta)_3(cpa)$ is possible due to the observation of about 0.66 wt % of N in the ZSM-5−$Eu(tta)_3(cpa)$ sample.

Luminescent Properties. ***Luminescence Spectra.*** It is illustrated in Figure 4A−E the excitation (left) and emission (right) spectra of matrix−$Eu(tta)_3(cpa)$ and isolated Eu^{3+} complexes as solids at room temperature. The excitation spectra of all samples, which were obtained by monitoring at 612 nm, exhibit a broad excitation band (BEB) between 250 and 450 nm. The broad excitation band can be assigned to the $\pi-\pi^*$ electron transition of the ligands, i.e., tta and cpa. Peaks observed at 396 and 467 nm in the excitation spectra of $Eu(tta)_3(H_2O)_2$ (Figure 4D) and $Eu(tta)_3(cpa)$ (Figure 4E) can be ascribed to the f−f transitions ($^7F_0 \rightarrow {}^5L_6$ and $^7F_0 \rightarrow {}^5D_2$) of Eu^{3+} ion, respectively. These weaker transitions in comparison with the ligand absorption are overlapped by BEB, proving that luminescence sensitization via excitation of the ligands is much more efficient than the direct excitation of the Eu^{3+} ion absorption level. In the emission spectra of all samples (except for the ZSM-5−$Eu(tta)_3(cpa)$), only characteristic emission of Eu^{3+} is detected, which indicates that the energy transfer from ligands to central ion Eu^{3+} (antenna effect) seems very efficient in both matrix−$Eu(tta)_3(cpa)$ and pure complexes. The relatively strong absorption of Eu^{3+} in the excitation spectrum of ZSM-5−$Eu(tta)_3(cpa)$ (Figure 4C, some peaks especially the peaks between 475 and 500 nm may be due to lines of the xenon lamp) and the emission of the ligand (400−550 nm) in the emission spectrum may prove the presence of incomplete complexes in the channels of ZSM-5.

Luminescence Decay Times. The $^5D_0$ emission decay curves were monitored at 612 nm under the excitation wavelength that maximizes the emission intensity. All these curves can be fitted by mono-, bi-, or triexponential functions. The fitting data are presented in Table 1, including lifetime values of $^5D_0$ levels of Eu^{3+} ions and the corresponding relative weightings for each

TABLE 1: Photoluminescent Data of Matrix−Eu(tta)$_3$(cpa) Samples and Isolated Europium Complexes in Solids[a]

	Atta−Eu(tta)$_3$(cpa)	MCM-41−Eu(tta)$_3$(cpa)	ZSM-5−Eu(tta)$_3$(cpa)	Eu(tta)$_3$(H$_2$O)$_2$	Eu(tta)$_3$(cpa)[b]
τ_1 (ms)	0.081 (7%[c])	0.249 (50%)	0.080 (7%)	0.247 (100%)	0.242 (22%)
τ_2 (ms)	0.314 (49%)	0.672 (50%)	0.358 (73%)		0.527 (78%)
τ_3 (ms)	0.829 (44%)		0.896 (20%)		
$\langle\tau\rangle$ (ms)	0.522	0.479	0.405	0.247	0.464
k_r (ms^{-1})	0.631	0.588	0.354	0.872	0.828
k_{nr} (ms^{-1})	1.284	1.498	1.891	3.177	1.325
n_w	0.3	0.6	1.2	2.0	0.2
q (%)	33.0	28.2	15.8	21.5	38.5

[a] The lifetimes (τ), average lifetimes ($\langle\tau\rangle$), radiative (k_r) and nonradiative (k_{nr}) decay rates, the numbers of water molecules in the first coordination sphere (n_w), and the emission quantum efficiency (q) of the $^5D_0$ Eu^{3+} excited state were obtained at room temperature. [b] Value obtained at the excitation of 350 nm. [c] Lifetimes (τ) and corresponding relative weightings.

species. The results indicate that more than one kind of symmetrical site of Eu^{3+} ion exists in these solid samples except for Eu(tta)$_3$(H$_2$O)$_2$ and that some Eu^{3+} ions in the composites form ternary complexes compared to Eu(tta)$_3$(cpa). For Eu(tta)$_3$(H$_2$O)$_2$, the obtained $^5D_0$ lifetime value was compatible with the reported values of 0.190[32] and 0.340 ms.[7] The luminescence decay curve of Eu(tta)$_3$(cpa) in solid adapts to biexponential functions, whereas a monoexponential (0.959 ms) can be adapted in an ether solution. The shortening lifetimes of Atta−Eu(tta)$_3$(cpa) (0.081 ms) might give rise to the quenching of O−H oscillators on the matrix surfaces to some absorbed Eu(tta)$_3$(H$_2$O)$_2$. The prolonged lifetimes of ZSM-5−Eu(tta)$_3$(cpa) emission (0.358 and 0.896 ms) due to the presence of attached Eu(tta)$_3$(cpa) agree with the observation of N content in the sample.

Emission Quantum Efficiencies (q). Following the method described in literature,[33] $^5D_0$ quantum efficiency (q) of the composites can be estimated when the luminescence data (emission spectra and $^5D_0$ lifetimes) presented above are employed. Assuming that only nonradiative (k_{nr}) and radiative (k_r, estimated according to the reported method,[33] shown in Table 1) processes are involved in the depopulation of the $^5D_0$ state, q may be expressed as

$$q = \frac{k_r}{k_r + k_{nr}}$$

Since the multiexponential decay curves which are usually observed in solid samples[34−36] can be attributed to the highly heterogeneous environments for the complexes in the solid surfaces, the average lifetime $\langle\tau\rangle$ is estimated by[36]

$$\langle\tau\rangle = \frac{\sum A_i\tau_i^2}{\sum A_i\tau_i}$$

where A_i are the preexponential factors related to the statistical weights of each exponential and τ_i represent the lifetimes of each exponential decay. We propose that the average lifetime ($\langle\tau\rangle$), radiative (k_r), and nonradiative (k_{nr}) transition rates may be related to the following equation:

$$k_r + k_{nr} = \frac{1}{\langle\tau\rangle}$$

The values found for q (%), average lifetimes ($\langle\tau\rangle$), and radiative (k_r) and nonradiative (k_{nr}) decay rates for all samples are shown in Table 1. The emission quantum efficiencies

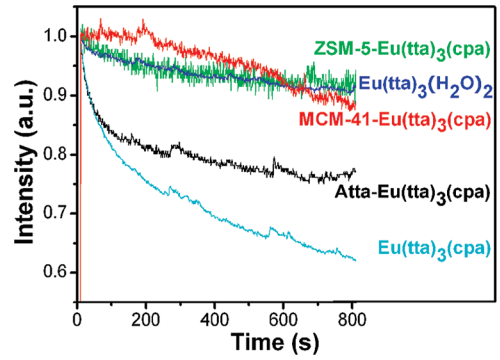

Figure 5. Photoluminescent stability of matrix−Eu(tta)$_3$(cpa) and the isolated Eu^{3+} complexes (normalized intensities of the $^5D_0 \rightarrow {}^7F_2$ transition as a function of time).

estimated for Atta−Eu(tta)$_3$(cpa) (33%) and MCM-41−Eu(tta)$_3$(cpa) (28%) are lower than Eu(tta)$_3$(cpa) (38%) but higher than Eu(tta)$_3$(H$_2$O)$_2$ (22%), indicating that the water molecules of Eu(tta)$_3$(H$_2$O)$_2$ were replaced by cpa and ternary complexes thus formed. The lower q value for MCM-41−Eu(tta)$_3$(cpa) compared with Atta−Eu(tta)$_3$(cpa) may result from the aggregates of Eu(tta)$_3$(H$_2$O)$_2$ inside the channels of MCM-41. We deduce that the incomplete complexes and the resulting higher intensity of the nonradiative process of the Eu^{3+} complex in ZSM-5−Eu(tta)$_3$(cpa) lead to a low quantum efficiency of about 16%.

The removal of water molecules from the Eu^{3+} coordination sphere of the Eu^{3+} complexes may be further studied. On the basis of the empirical formula suggested by Supkowski and Horrocks,[37] it is a possibility to estimate the number of water molecules (n_w) coordinated to the metal ion in the matrixes with the following formula:

$$n_w = 1.11(k_{nr} - k_r - 0.31)$$

It should be noted that n_w values do not represent a single molecule here since the composites contain two or three local environments of Eu^{3+} ions, but they are considered as a whole. Agreeing with the assumed formation of the complexes in composites, the results (Table 1) indicated that some water molecules in the Eu(tta)$_3$(H$_2$O)$_2$ complex were removed from the Eu^{3+} first coordination shell after being added to the matrix−cpa or pure cpa.

Stability. ***Photoluminescent Stability.*** To compare photoluminescent stability, kinetic scans of luminescence induced by UV light (350 nm) for the different samples were carried out. Figure 5 demonstrates the dependence of the normalized emission intensity of the $^5D_0 \rightarrow {}^7F_2$ transition (612 nm) on irradiation time for different samples. A decline of the emission

intensity of the $^5D_0 \rightarrow {}^7F_2$ transition with increasing exposure time is observed in both matrix- and isolated Eu^{3+} complexes. Evidently the decrease of the emission intensities of Atta−$Eu(tta)_3(cpa)$ resembles that of pure $Eu(tta)_3(cpa)$, indicating similar environments of Eu^{3+} ions in the two samples. It is understandable that the decay curve for MCM-41−$Eu(tta)_3(cpa)$ presents higher stability because of the shielding effect of the walls around the embedded Eu^{3+} complexes. The rapid diminishment of $Eu(tta)_3(cpa)$ complexes may be created by the decomposition of $Eu(tta)_3(cpa)$ to more stable $Eu(tta)_3(H_2O)_2$ with a inferior luminescence, suggesting a UV-sensitive interaction of the ligand cpa with the central Eu^{3+} ions.

Thermal Stability. The stability of matrix- and isolated $Eu(tta)_3(cpa)$ complexes were further studied by the TG and DTG measurement. As the DTG curves show (Figure S4, see the Supporting Information), the thermal stability of the isolated complex (256 °C for $Eu(tta)_3(H_2O)_2$ and 326 °C for $Eu(tta)_3(cpa)$ decomposition) is enhanced by loading in matrix (481 °C on Atta, 340 and 492 °C on MCM-41). We suggest that the two peaks in the DTG curves of MCM-41−$Eu(tta)_3(cpa)$ agree with the assumed formations in the pores of MCM-41 (binary Eu^{3+} complexes and ternary Eu^{3+} complexes simultaneously). Shielding effect of MCM-41 in MCM-41−$Eu(tta)_3(cpa)$ in comparison with Atta−$Eu(tta)_3(cpa)$ complex can be ignored. The thermal stability of Eu^{3+} complexes seems similar to the isolated $Eu(tta)_3(H_2O)_2$ because of the complication in ZSM-5. In addition, three types of water in agreement with the literature[20] are observed in Atta−$Eu(tta)_3(cpa)$ samples, which are free pore water and water adsorbed on surfaces (57 °C), zeolitic water (173 °C), and structural water (365 °C).

To further study their thermal stability, the samples were heated at specific temperature (120−240 °C) for 30 min, and their relative luminescence intensities were recorded. The plot of intensities at 612 nm to related heating temperature (Supporting Information Figure S5) proves that the stability of binary complex was improved after it was introduced to the matrixes, especially attapulgite. Besides, these curves might support the assumed formations of the complexes in the hosts, e.g., the direct drop of the luminescence of MCM-41−$Eu(tta)_3(cpa)$ may suggest the presence of $Eu(tta)_3(H_2O)_2$.

Conclusions

In this study, we had successfully linked a europium complex with three matrixes via a ligand exchange reaction. The obtained samples of Atta−$Eu(tta)_3(cpa)$, MCM-41−$Eu(tta)_3(cpa)$, and ZSM-5−$Eu(tta)_3(cpa)$ were characterized by ^{29}Si MAS NMR, CHN elemental analysis, ICP for Eu^{3+} contents, XRD, and UV−vis absorption spectra. The results led us to a conclusion that Eu^{3+} complexes were covalently bonded onto the outer surfaces of Atta, or to the inner walls of the pores of MCM-41, whereas they invaded into the channels of ZSM-5 after decomposition. Some free binary complexes were also trapped in the channels due to the relatively small pores of MCM-41. The assumed microstructures of the composites were confirmed by the investigation on their luminescence and stability. The luminescence efficiency and coordinated waters of the Eu^{3+} complexes for composites and their stability under heat or UV light were also studied. As the data suggested, the composites in comparison with the isolated complexes generally resulted in more efficient emission, and also possessed much higher thermal stability and exposure durability, since the matrixes interacted strongly with europium complexes. It should be emphasized that complexes bonded to attapulgite were superior to that introduced to the other matrixes, not only for the natural availability of the clay, but also for its stronger luminescence and similar stability. The europium-complex-bonded attapulgite appears an interesting material for photophysical applications.

Acknowledgment. We are grateful to the National Natural Science Foundation of China (Project 20401008) and the program for New Century Excellent Talents in University (NCET-06-0902) for financial support.

Supporting Information Available: TEM images of Atta−APTES, elemental analysis, FTIR spectra, XRD patterns, TG/DTG curves, and temperature dependence of fluorescence intensity of matrix−$Eu(tta)_3(cpa)$ samples. This material is available free of charge via the Internet at http://pubs.acs.org.

References and Notes

(1) Kido, J.; Okamoto, Y. *Chem. Rev.* **2002**, *102*, 2357.
(2) Kuriki, K.; Koike, Y.; Okamoto, Y. *Chem. Rev.* **2002**, *102*, 2347.
(3) Binnemans, K.; Görller-Walrand, C. *Chem. Rev.* **2002**, *102*, 2303.
(4) Carlos, L. D.; Ferreira, R. A. S.; de Zea Bermudez, V.; Ribeiro, S. J. L. *Adv. Mater.* **2009**, *21*, 509.
(5) Stich, M. I. J.; Nagl, S.; Wolfbeis, O. S.; Henne, U.; Schaeferling, M. *Adv. Funct. Mater.* **2008**, *18*, 1399.
(6) Fernandes, M.; de Zea Bermudez, V.; Sá Ferreira, R. A.; Carlos, L. D.; Charas, A.; Morgado, J.; Silva, M. M.; Smith, M. J. *Chem. Mater.* **2007**, *19*, 3892.
(7) Li, H.; Inoue, S.; Machida, K. i.; Adachi, G. y. *Chem. Mater.* **1999**, *11*, 3171.
(8) Wada, Y.; Sato, M.; Tsukahara, Y. *Angew. Chem., Int. Ed.* **2006**, *45*, 1925.
(9) Xu, Q.; Li, L.; Liu, X.; Xu, R. *Chem. Mater.* **2002**, *14*, 549.
(10) Peng, C.; Zhang, H.; Yu, J.; Meng, Q.; Fu, L.; Li, H.; Sun, L.; Guo, X. *J. Phys. Chem. B* **2005**, *109*, 15278.
(11) Sun, L. N.; Zhang, H. J.; Peng, C. Y.; Yu, J. B.; Meng, Q. G.; Fu, L. S.; Liu, F. Y.; Guo, X. M. *J. Phys. Chem. B* **2006**, *110*, 7249.
(12) Yan, B.; Wang, Q.-M. *Cryst. Growth Des.* **2008**, *8*, 1484.
(13) Brunet, E.; Alhendawi, H. M. H.; Juanes, O.; Jiménez, L.; Rodríguez-Ubis, J. C. *J. Mater. Chem.* **2009**, *19*, 2494.
(14) Terazzi, E.; Suarez, S.; Torelli, S.; Nozary, H.; Imbert, D.; Mamula, O.; Rivera, J. P.; Guillet, E.; Bénech, J. M.; Bernardinelli, G.; Scopelliti, R.; Donnio, B.; Guillon, D.; Bünzli, J. C. G.; Piguet, C. *Adv. Funct. Mater.* **2006**, *16*, 157.
(15) Pumera, M.; Cabala, M.; Veltruská, K. n.; Ichinose, I.; Tang, J. *Chem. Mater.* **2007**, *19*, 6513.
(16) Lezhnina, M.; Benavente, E.; Bentlage, M.; Echevarría, Y.; Klumpp, E.; Kynast, U. *Chem. Mater.* **2007**, *19*, 1098.
(17) Augsburger, M. S.; Pedregosa, J. C.; Strasser, E.; Perino, E.; Mercader, R. C. *J. Phys. Chem. Solids* **1998**, *59*, 175.
(18) Van Olphen, H. *Science* **1966**, *154*, 645.
(19) José-Yacaman, M.; Rendon, L.; Arenas, J.; Serra Puche, M. C. *Science* **1996**, *273*, 223.
(20) Chiari, G.; Giustetto, R.; Druzik, J.; Doehne, E.; Ricchiardi, G. *Appl. Phys. A: Mater. Sci. Process.* **2008**, *90*, 3.
(21) Tetsuka, H.; Ebina, T.; Tsunoda, T.; Nanjo, H.; Mizukami, F. *Nanotechnology* **2007**, *18*, 355701.
(22) Melo, D. M. A.; Ruiz, J. A. C.; Melo, M. A. F.; Sobrinho, E. V.; Schmall, M. *Microporous Mesoporous Mater.* **2000**, *38*, 345.
(23) Celedon, S.; Quiroz, C.; Gonzalez, G.; Sotomayor Torres, C. M.; Benavente, E. *Mater. Res. Bull.* **2009**, *44*, 1191.
(24) Sánchez, A.; Echeverría, Y.; Torres, C. M. S.; González, G.; Benavente, E. *Mater. Res. Bull.* **2006**, *41*, 1185.
(25) Alvaro, M.; Fornés, V.; García, S.; García, H.; Scaiano, J. C. *J. Phys. Chem. B* **1998**, *102*, 8744.
(26) Dörwald, F. Z. *Organic Synthesis on Solid Phase*; Wiley-VCH Verlag GmbH: Weinheim, Germany, 2002; p 7.
(27) Cai, Q.; Lin, W.-Y.; Xiao, F.-S.; Pang, W.-Q.; Chen, X.-H.; Zou, B.-S. *Microporous Mesoporous Mater.* **1999**, *32*, 1.
(28) dos Santos, C. M. G.; McCabe, T.; Gunnlaugsson, T. *Tetrahedron Lett.* **2007**, *48*, 3135.
(29) Smith, G. F.; Cagle, F. W. *J. Org. Chem.* **1947**, *12*, 781.
(30) Melby, L. R.; Rose, N. J.; Abramson, E.; Caris, J. C. *J. Am. Chem. Soc.* **1964**, *86*, 5117.
(31) Kaiser, E.; Colescott, R. L.; Bossinger, C. D.; Cook, P. I. *Anal. Biochem.* **1970**, *34*, 595.
(32) Lenaerts, P.; Driesen, K.; VanDeun, R.; Binnemans, K. *Chem. Mater.* **2005**, *17*, 2148.

(33) Carlos, L. D.; Sá Ferreira, R. A.; de Zea Bermudez, V.; Ribeiro, S. J. L. *Adv. Funct. Mater.* **2001**, *11*, 111.
(34) Wen, X.; Li, M.; Wang, Y.; Zhang, J.; Fu, L.; Hao, R.; Ma, Y.; Ai, X. *Langmuir* **2008**, *24*, 6932.
(35) Hagerman, M. E.; Salamone, S. J.; Herbst, R. W.; Payeur, A. L. *Chem. Mater.* **2003**, *15*, 443.
(36) Martínez Martínez, V.; López Arbeloa, F.; Bañuelos Prieto, J.; López Arbeloa, I. *J. Phys. Chem. B* **2005**, *109*, 7443.
(37) Supkowski, R. M.; Horrocks, W. D. *Inorg. Chim. Acta* **2002**, *340*, 44.

JP906848E